Int. J. Heat Mass Transfer. Vol. 25, No. 9, pp. 1397–1409, 1982
Printed in Great Britain

0017–9310/82/091397–13 $03.00/0
Pergamon Press Ltd.

MEASUREMENTS OF INSTABILITY AND DISTURBANCE GROWTH IN VERTICAL BUOYANCY INDUCED FLOWS IN COLD WATER

J. M. HIGGINS
Eastman Kodak Company, Rochester, New York, U.S.A.
and
B. GEBHART
University of Pennsylvania, Department of Mechanical Engineering and Applied Mechanics
Philadelphia, PA 19104, U.S.A.

(*Received* 30 *March* 1982)

Abstract—An experimental study of the stability of buoyancy induced flow of cold water, adjacent to a vertical isothermal surface has been carried out. A tall surface was designed and constructed to achieve an isothermal surface condition, for use in cold water. The experiment was conducted for conditions near the density extremum, at parameter values around $R = 0$, 0.1 and 0.4, with a temperature difference $(t_0 - t_\infty)$ limited to 5°C. Linear stability calculations had previously been carried out for these conditions. Base flow and disturbance temperatures and velocities were measured with a fine thermocouple probe and a hot film anemometer. For the two upflow circumstances, $R = 0$ and $R = 0.1$, measured disturbance amplitude data agree well with the linearly computed disturbance profiles. For $R = 0$, disturbance activity first arises and propagates downstream at a frequency slightly higher than that predicted by linear calculations to be the most quickly amplified, or 'favored', frequency. For $R = 0.1$, the measured characteristic frequencies are slightly below the calculated favored frequency. As transition arises and proceeds, a broadening range of frequencies is found. Disturbances at $R = 0.1$ arise sooner and are more vigorous than those observed at $R = 0$, in accordance with linear theory.

Systematic measurement problems were encountered for $R = 0.4$, for which $t_0 \approx 6.6$ and $t_\infty \approx 2.3$°C. For these conditions, the outer part of the thermal boundary layer is below the extremum temperature, with a buoyancy force reversal occurring. Measured disturbance frequencies were slightly higher than the calculated favored frequency.

Burst activity signaled the beginning of transition in several of the tests performed. The location and vigor of this activity corresponds well with the values of the predictive parameters E and Q_{BT}, proposed by Jaluria and Gebhart *J. Fluid Mech.* **66**, 309–337 (1974) and by Mahajan and Gebhart *J. Fluid Mech.* **91**, 131–154 (1979). The experimental values of E and Q_{BT} determined here are slightly lower than those previously reported. This indicates the presence of an enhanced instability and amplification mechanism operating in cold water, in terms of the kinds of parameters which appear in E and Q_{BT}.

NOMENCLATURE

B, dimensionless frequency, independent of G;
E, kinetic energy flux parameter to correlate beginning of transition;
$E(U,t_\infty)$, anemometer output voltage, a function of both ambient velocity and temperature;
E_0, zero velocity anemometer output voltages;
g, acceleration of gravity;
G, $4(Gr_x/4)^{1/4}$;
G^*, a uniform surface flux value;
Gr, Grashof number;
k, thermal conductivity;
p, pressure [bars];
Pr, Prandtl number;
$q,q(s,p)$, salinity and pressure dependent exponent of the temperature term appearing in the density relation;
q'', heat flux;
Q_{BT}, parameter used to correlate beginning of transition;
R, parameter indicating location of system temperatures t_0 and t_∞ with respect to the density extremum temperature t_m;
s, salinity [ppt];
t, local boundary layer temperature [°C];
t_f, boundary layer film temperature, the average of t_0 and t_∞;
t_m, temperature at which maximum density occurs for a given salinity and pressure [°C];
t_0, temperature of test surface [°C];
t_∞, temperature of ambient medium [°C];
Δt, $t_0 - t_\infty$[°C];
$T(\eta)$, dimensionless boundary layer temperature;
$u(x,y)$, parallel component of velocity;
U, fluid velocity;
x, downstream coordinate;
y, normal coordinate.

Greek symbols

α,	a parameter in the density relation in ref. [8];
$\eta(x,y)$,	similarity variable;
μ,	absolute viscosity;
ν,	kinematic viscosity.

1. INTRODUCTION

EXPERIMENTS in a pressurized gas [3] have verified the existence of a neutral curve in an interferometric study of a vertical constant flux surface. Artificially imposed disturbances were found to amplify most in the outer region of the boundary layer. A later study [4] then determined the consequences of a thermal storage effect in the boundary condition for a constant flux surface. They also experimented with a water-like silicone fluid ($Pr = 7.7$) detecting the naturally occurring 'first bursts' which signal the start of transition. A selective frequency amplification mechanism was postulated to explain the observed concentration of disturbances within a very narrow frequency band. Extensive calculations [5] resulted in coupled neutral stability curves as well as disturbance amplification contours for a constant flux surface for $Pr = 7.7$. Very highly selective amplification was predicted. Temperature and velocity disturbance amplification rates were measured and the favored frequency hypothesis was further supported. A simplified numerical technique was used [6] to compute neutral curves and detailed amplification contours for a constant flux surface for a wide range of Prandtl numbers.

The experimental investigation in water [1] of the downstream propagation of disturbances through transition was conducted at room temperature. The disturbance frequencies in the upstream laminar portion of a flow undergoing transition were found to be remarkably close to the favored ones predicted by analysis. The frequencies dominating the downstream turbulent flow were slightly higher. These results also indicated that velocity transition occurs first, followed shortly by thermal transition. Related to this delayed thermal transition, the frequencies of the temperature disturbances were always less than those of the velocity disturbances. The first appearance of turbulent bursts was found to be an accurate and reliable indicator of the beginning of transition. The kinetic energy flux parameter

$$E = G^* \left(\frac{\nu^2}{gx^3}\right)^{2/15},$$

discussed in Appendix 1, closely correlates the beginning of transition for the data. It also correlates the observations of previous investigators reasonably well.

The experiments in ref. [2] determined transition limits in pressurized nitrogen. The indicated 'beginning of transition' parameter was

$$Q_{BT} = \left(\frac{g''}{g\mu}\right)^{1/5} \left(\frac{gx^3}{\nu^2}\right)^{2/15},$$

also discussed in Appendix 1. It is a more general correlation, applying to gases as well as to liquids. In the most recent study of stability [7] a constant heat flux surface generated the flow in cold water, at 4°C. The results indicate a frequency favoring mechanism that is less sharp for cold water. The velocity and thermal transition appeared to occur simultaneously.

This study concerned the stability of a buoyancy induced flow in cold water adjacent to a vertical isothermal surface, for several ambient temperature levels t_∞. A surface was designed and constructed to be isothermal in a cold water ambient. The experiments were conducted for several different values of the temperature parameter

$$R = \frac{(t_m - t_\infty)}{(t_0 - t_\infty)},$$

which is a convenient indicator of the location of system temperatures t_0 and t_∞, with respect to t_m. Values of $R = 0$, 0.1 and 0.4 were tested, with a temperature difference $(t_0 - t_\infty) \simeq 5$°C. The test conditions are summarized in Table 1.

Using a fine thermocouple probe, mounted together with a hot film anemometer probe, frequency and amplitude data for both temperature and velocity disturbances were obtained. Data were taken across the boundary region, at several values of the similarity variable η, for each vertical position traversed. Disturbance amplitudes and frequencies are compared to computations from linear stability theory. Deviations are noted and discussed for all the experimental temperature conditions. The local relative status of transition is noted and compared with the parameters marking the beginning of transition which were suggested by previous investigators.

Uncertainties regarding the operation of the hot film anemometer in the region $t < t_m$ arose in the course of the measurements at the $R = 0.4$ condition. These are discussed in section 3.2.

2. THE EXPERIMENT

2.1. *Apparatus*

Experimental studies of buoyancy induced boundary layer flows in water have largely been carried out with constant heat flux surfaces. Such a boundary condition may be achieved by supplying a carefully controlled electric current to a thin and uniformly electrically conductive surface. This results in a heat flux at the solid boundary that is independent of the vertical coordinate x. The resulting wall temperature, or $t_0(x) - t_\infty$, varies as $x^{1/(4+q)}$, in cold water, where q is the exponent of the temperature term appearing in the density relation in ref. [8].

On the other hand, maintaining an isothermal condition along a surface requires a heat flux at the solid–liquid boundary which varies as $x^{-1/4}$, as determined from laminar boundary layer theory. This variation is particularly steep in the small x, or leading

Table 1. Temperature conditions for measurements taken

Test	t_0 (°C)	t_∞ (°C)	B*	R	G	E†	Q_{BT}†
1	9.14	4.18	+	−0.03	207		
2	9.14	4.18	+	−0.03	275		
3	9.02	4.10	+	−0.01	275		
4	9.02	4.10	+	−0.01	297		
5	9.07	4.08	+	−0.01	378	12.2	316.6
6	9.07	4.08	+	−0.01	417	12.8	332.7
7	9.05	4.15	+	−0.03	338		
8	9.47	3.31	+and−	0.12	304		
9	9.47	3.31	+and−	0.12	385	12.8	321.9
10	8.59	3.41	+and−	0.12	378		
11	8.59	3.41	+and−	0.12	417	14.1	352.8
12	6.56	2.31	+and−	0.40	414		
13	6.68	2.31	+and−	0.39	448		

* B indicates the direction of the buoyancy force, determined by values of t_0, t_∞, and t_m.
† Summary of values of the kinetic energy flux parameter E, and beginning of transition parameter Q_{BT}, for tests exhibiting 'bursts'.

edge area. It becomes more gradual as x increases. Achieving an experimental surface with an $x^{-1/4}$ heat flux variation, resulting in an isothermal surface condition, was the goal of the design effort. For all experiments t_0 was greater than t_∞, thereby heating the ambient water.

A forced flow water heat exchange concept was found to fit the needs of this application particularly well. A Plexiglas heat exchanger chamber, connected to the backside of a 0.635 cm thick copper test surface, is shown schematically in Fig. 1. It was carefully designed to achieve an isothermal condition on the test surface side in contact with the ambient medium. Heated water enters the chamber at the bottom, flows upward the length of the test surface, and leaves at the top. The combination of the entrance length effect in the leading edge region, coupled with a careful choice of other heat exchange parameters, such as flow rate and flow passage geometry, was found to closely produce the desired local heat flux variation with x, downstream on the test surface.

The completed apparatus is shown in Fig. 2(a) and (b). The test surface has been mounted on a stainless steel angle-iron frame provides additional rigidity, as well as support for final positioning in the experiment. A 3-dim. traverse mechanism, supporting the velocity and temperature boundary layer probes, is attached to this frame. This mechanism allows the whole structure to hang in place from the top of the large stainless steel vessel containing the ambient medium. The diagonals permit the adjustment to a vertical position in the ambient medium.

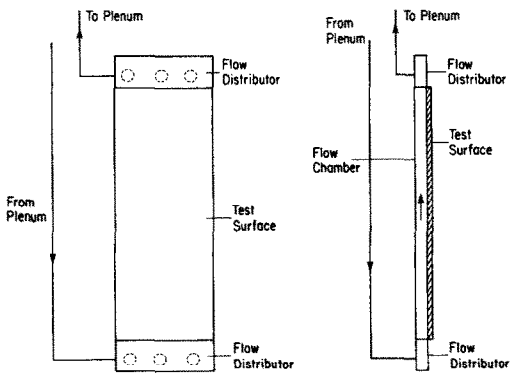

FIG. 1. Front and side views of test surface and flow chamber assembly.

All Plexiglas surfaces, as well as plumbing, were carefully insulated with a flexible foam elastomeric insulation, attached to the structure with stainless steel safety wire. A special A-frame structure was built to insure careful handling of the test surface. Figure 3(a) shows a crane at the apex of the gantry, providing easy lifting capability. Casters allow the whole structure to be moved into place straddling the large tank, as in Figs. 3(b) and (c). The test surface is carefully lowered and positioned in the ambient medium. The gantry is then used as a support structure for the heat exchanger plumbing, as seen in Fig. 3(d).

The detailed results of the recent stability calculations and experiments in cold water reported previously [7] provided valuable insight into the choice of parameters for the design of this test surface. An estimate was made of the downstream length required to achieve disturbance amplification, with the isothermal surface condition, of vigor comparable to that observed adjacent to uniform flux surfaces. Also, order of magnitude estimates were made regarding time scales for the test surface heating transient, the base flow starting transient, and the resulting ambient medium temperature stratification rate. A detailed heat transfer analysis for the test surface assembly was carried out. A brief structural analysis of both the heat exchanger assembly and flow system indicated that it was sufficiently strong and rigid. Details of these computations can be found in ref. [9].

2.2. *Hot film calibration*

All velocity measurements were taken with a con-

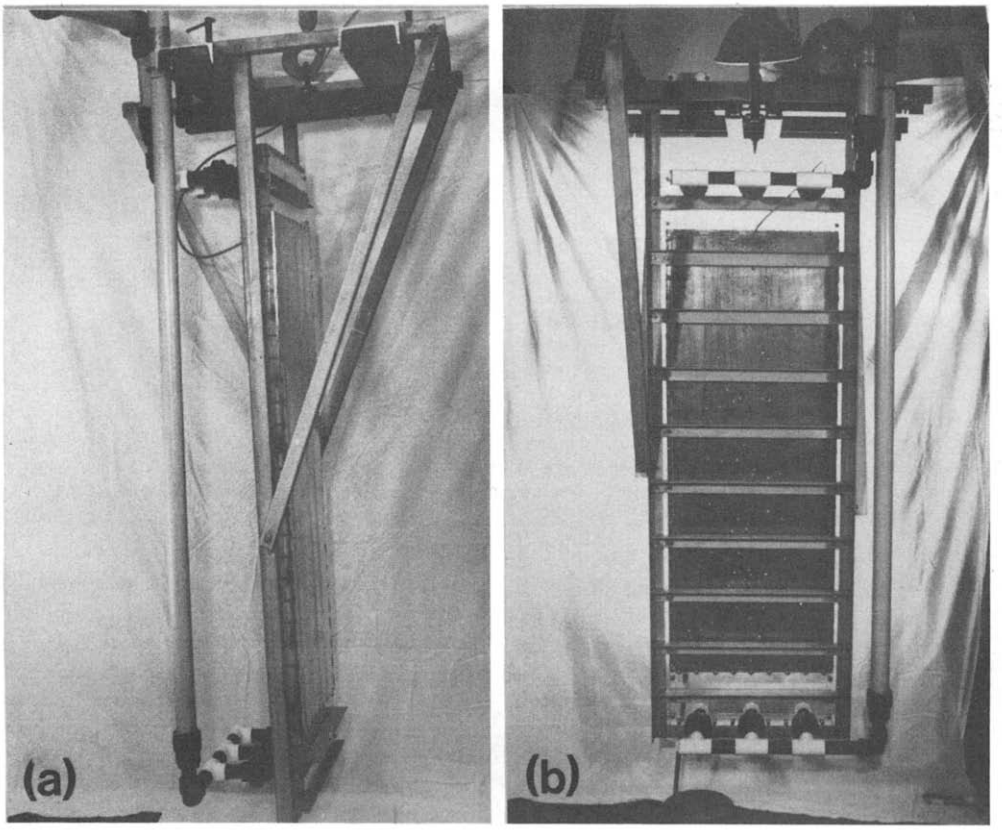

FIG. 2. Side and back views of isothermal surface assembly.

stant temperature anemometer (CTA), Disa 55M01, with a fiber film probe, type 55R14. This probe has a protective quartz coating, making it suitable for stable use in water. The probe diameter is 90 μm and the active length is 1.25 mm. All probe holder and cable junctions were carefully sealed with silicone cement, for immersion in water. A warm-up time for all electronics of at least 1 h was allowed to assure stable operation. The probe temperature was maintained at 28°C throughout the calibration and all measurements.

The calibration apparatus has already been described in detail [10]. The voltage output of the CTA is a function of both the temperature and velocity of the surrounding medium. The calibration tank water was maintained at a known temperature, while traversing the probe at known speeds vertically downward through the fluid, in the range from 0.08 to 5.0 cm^{-1}. The expected velocities lay in the lower part of this range. Calibration was repeated for four different ambient temperature conditions from 1.3 to 10°C, resulting in a family of four curves. The zero velocity voltage, E, is plotted in Fig. 4, as a function of ambient temperature, t_∞. Error bars indicate the range of E readings obtained during the calibration procedure, at each temperature. The four calibration curves $(E - E_0)$, one for each ambient temperature condition, are in Fig. 5. The curves are consistent throughout the velocity range, even at the low velocities critical to the measurements made in this study.

Some anomalous behavior arose in the low temperature calibration, $t = 1.3$°C. A slow and periodic drift was sometimes observed in the E_0 readings. A relatively long waiting period was required between velocity data points, to allow this drift to decrease and produce consistent, smooth results. This behavior is thought to be a consequence of a buoyancy force reversal within the plume generated by the hot film probe. Since the temperature ranged from 1.3 to 28°C within the plume, the extremum condition was present. This behavior was observed only for the 1.3°C calibration. This is discussed further in section 3.2.

The zero velocity voltage data in Fig. 4 was approximated well with a second order polynomial. The calibration curves were fitted to an eighth order polynomial, of the form $U = f(E - E_0)$. In the actual measurements, a copper–constantan thermocouple junction, 0.076 mm in diameter, adjacent to the hot film, recorded the local boundary layer temperature. A Lagrange interpolation scheme, using the temperature at each location, along with the CTA voltage output, determined the velocity at each measurement location.

2.3. *Experimental procedure*

The ambient water used throughout the measure-

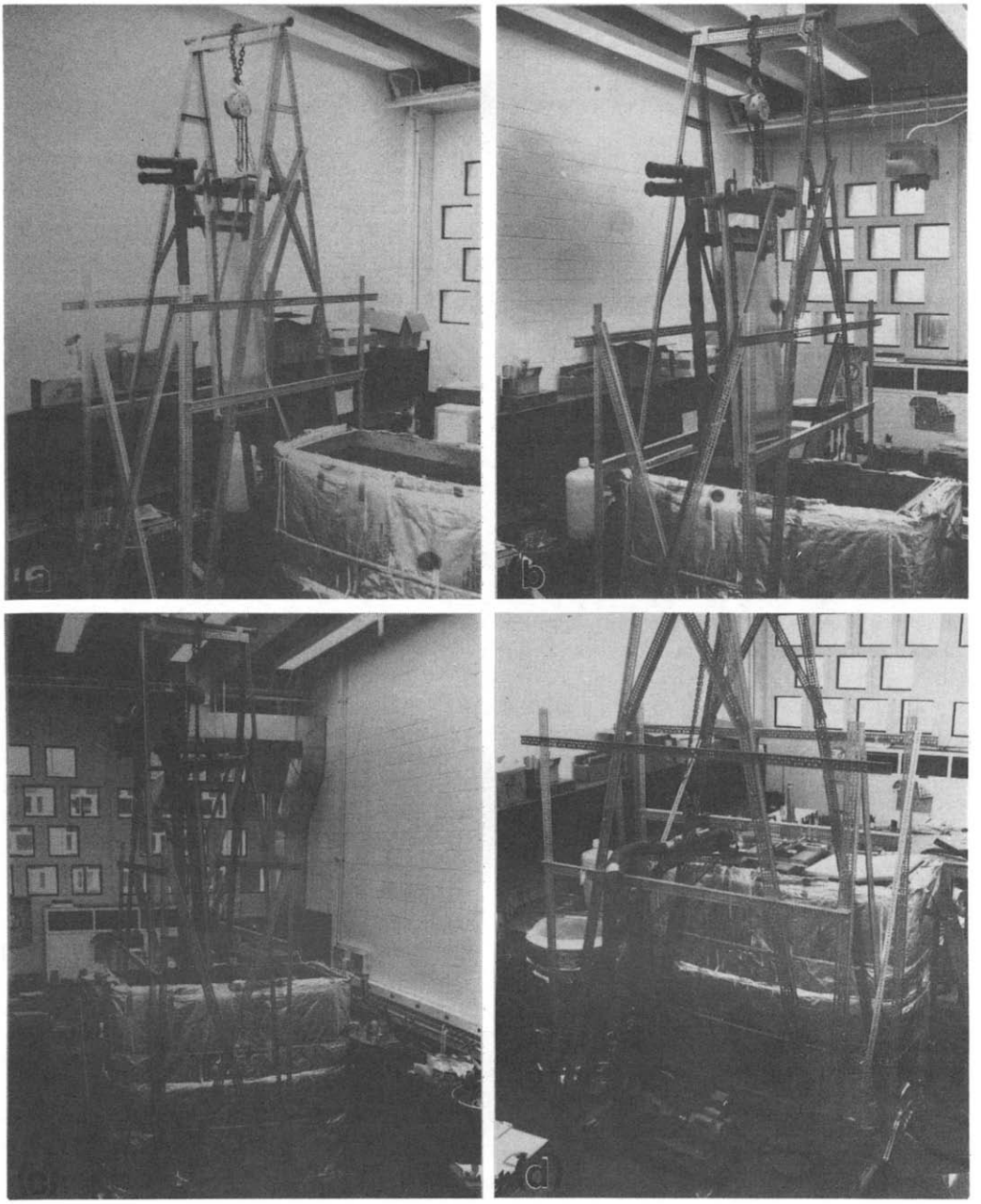

FIG. 3(a)–(d). Sequence showing test assembly lifting mechanism, placement of assembly into tank, and final setup.

ments was carefully degassed to assure that no bubble formation would occur on the hot film surface during operation. For each test, the ambient medium was chilled and thoroughly stirred. It was then allowed to settle for 1 h before measurements began. A vertical array of four thermocouples was monitored to insure that no stratification had arisen. The maximum allowable test time, before appreciable stratification occurred, was found to be 45–60 min. Stratification resulted from the accumulation of warm boundary layer fluid from the test surface, at the top or at the bottom of the tank.

The probes were traversed with an accurate, 3-dim. traverse mechanism. Thermocouple and CTA voltage output were recorded with a Beckman R511 Dynagraph chart recorder. Excellent amplification was achieved at 0.1 $V\,cm^{-1}$ for the CTA output, and 0.05 $mV\,cm^{-1}$ for the thermocouple output. The signals were centered on the scales at these high amplifications, making even small distrubances accurately readable. The absolute voltage levels were read from a Hewlett–Packard 5328A Universal Counter. This counter was also used throughout the measurements to check for chart-recorder drift.

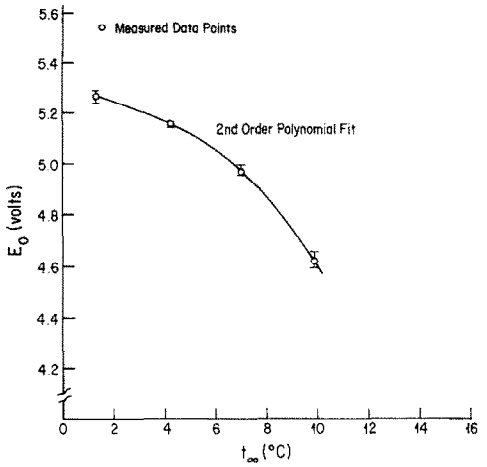

FIG. 4. Zero velocity voltage E_0 as a function of ambient temperature t_∞. Probe sensor temperature 28°C.

3. EXPERIMENTAL RESULTS AND CONCLUSIONS

3.1. *Introduction*

The previous experimental investigation [1] of the propagation of disturbances all the way downstream through transition, was in room temperature water. The appearance of turbulent bursts was found to be an accurate and reliable experimental indicator of the beginning of transition. The kinetic energy flux parameter

$$E = G^* \left(\frac{v^2}{gx^3}\right)^{2/15},$$

discussed in Appendix 1, closely correlated the beginning of transition for that data, as well as some previous data. The similar investigation in pressurized nitrogen [2] determined the following parameter to predict the beginning of transition:

$$Q_{BT} = \left[\frac{q''}{g\mu}\right]^{1/5} \left[\frac{gx^3}{v^2}\right]^{2/15}.$$

This is a more general correlation, applying to gases as well as liquids. The most recent reported study of stability [7], in cold water with a constant heat flux surface, indicated a less sharp selective amplification

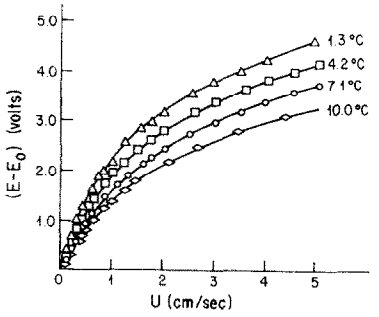

FIG. 5. Anemometer output voltage as a function of velocity U, for four ambient temperatures. Probe sensor temperature 28°C.

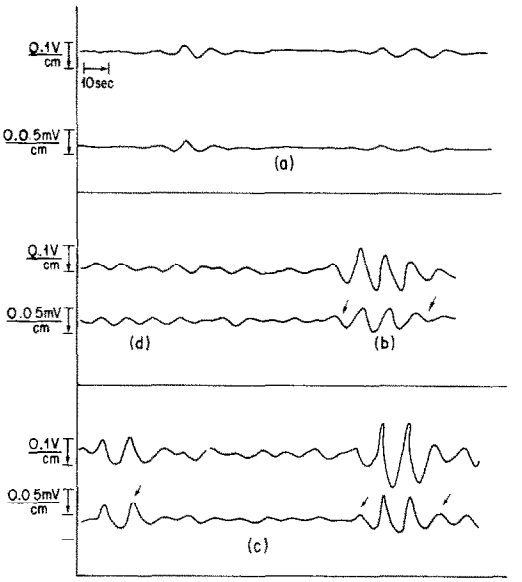

FIG. 6. Velocity and temperature disturbance traces, illustrating four categories of disturbance frequencies: (a) principal, (b) predominant, (c) large NL, (d) small NL. Upper traces are anemometer output, lower are thermocouple output.

mechanism in cold water, as well as simultaneous velocity and thermal transition.

In the present study, the occurrence of turbulent bursts was also used as the indicator of the beginning of transition. Fundamentally, four types of disturbance activity have been categorized and analyzed here: (1) principal, (2) predominant, (3) large non-linear, and (4) small non-linear disturbances. Figures 6 (a)–(d) are some actual experimental traces, illustrating these four categories. The 'principal' frequencies are well-defined, sinusoidal, small amplitude disturbances. They occur only in the laminar flow regions. The magnitudes of the principal frequency disturbances illustrated in Fig. 6 (a) are approximately 3% and 5% of the base flow velocity and temperature values, respectively. These disturbances are the ones expected to correspond closely with linear disturbance theory results. The 'predominant' frequencies, for example, Fig. 6(b), relate to the 'first bursts', signaling the start of transition. Both velocity and temperature disturbances shown here are approximately 10% of the base flow values. Large non-linear disturbances, which are not as sharply defined as bursts, but are likely the result, at least partially, of non-linear mechanisms, are considered separately. Very often, as indicated by the arrows in Figs. 6(b) and (c), such disturbances immediately preceded and followed bursts. The early part of the trace in Fig. 6(c) also shows the occurrence of these disturbances, independently of the following burst. The small amplitude non-linear disturbances, which occurred adjacent to non-linear and burst activity as seen in Fig. 6(d) were also considered separately.

The definitions of individual disturbances in these

last two categories are somewhat subjective. The disturbances are certainly combinations of different disturbance frequencies. The proper determination of a characteristic frequency was less clear for these than in the first two categories of disturbances.

Frequency data for both temperature and velocity disturbances were recorded at several values of η, and averaged across the layer, for each x location traversed. The principal disturbance amplitudes and frequencies are compared to computations from linear stability results in section 3.3. Frequencies from the remaining three disturbance categories are also compared to calculations. The deviations are discussed, for all temperature conditions tested.

3.2. *Qualitative aspects of the measurements*

The calculated and measured base flow, for test 1, are compared in Fig. 7. The agreement is very good, as expected at the relatively low value of $G = 207.22$. The computed maximum base flow velocity for these conditions is $u_{max} = 0.3808\ \text{cm s}^{-1}$. In this low velocity range, the results are very sensitive to even small electronic drift in the anemometer unit. It was determined that an error in E_0 of only 1.7%, can result in an error in velocity of 12%. Great care was taken to allow sufficient warm up time for all electronics before performing any test. Also, E_0 readings were carefully taken before and after a test, and compared to the calibration E_0 values. If necessary, a correction was then applied. In view of such sensitivity the data shown in Fig. 7 are in excellent agreement with theory.

The t_0, t_∞ condition in tests 8–11 each result in a narrow region in the thermal layer, at large η, where the fluid temperature is less than t_m. Thus, there is an outside buoyancy force reversal. In the course of the measurements, as the traverse progressed away from the surface, toward the cold ambient, the velocity probe detected a distinct, long wavelength meandering behavior. This was a more prominent feature at the lower G values, the less vigorous flow conditions. This behavior was not seen until the probes were out in water where the local temperature was less than t_m. Since the hot film probe was always at 28°C, the crossing of the density extremum is related to this meandering motion. In fact, in the recent experimental investigation of line-source plumes in cold water [11] observed a 'slow, periodic but laminar swaying of the plume', at all heat input levels tested. It is recalled that this same phenomenon was observed, at a smaller amplitude, during the probe calibration at $t = 1.37$°C. These motions were of largest magnitude in tests 12 and 13 for $R \simeq 0.4$, where a larger region of the thermal boundary layer was below t_m.

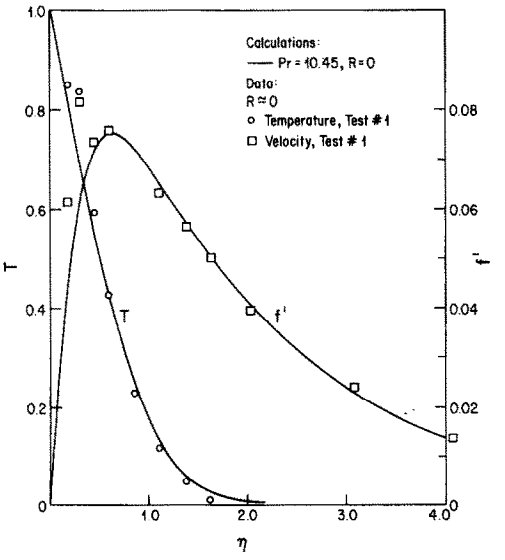

FIG. 7. Computed base flow velocity and temperature profiles for $R = 0$, $Pr = 10.45$. Data points are base flow results of test 1.

An additional feature of hot film response arose in the measurements at $R = 0.4$. The calibration was performed by moving the probe downward in the calibration tank, at an accurately known velocity. For the low temperature ambient, $t = 0.37$°C, the warm plume was, for the most part, upward flow. This flow is reinforced by the relative upward flow of the ambient fluid. However, for the conditions of the test at $R = 0.4$, the boundary layer is flowing downward, opposing the direction of the plume flow. If the magnitude of the plume velocity is appreciable compared to that of the surrounding base flow, the calibration method used may not be appropriate for the experiment at $R = 0.4$.

In order to assess these effects the maximum velocity in the plume caused by the hot film was computed, at a distance of five wire diameters above the probe. As computed from the base flow profile for $R = 0.4$, it was found to be about 15% of the maximum velocity in the boundary layer, a significant amount. Therefore, the calibration procedure may not be reliable for the condition $R = 0.4$. For this reason, only frequency information was processed from the hot film output.

A small amount of backlash was present in the traversing mechanism. It was necessary, for several test results, to make a small correction in η location to the data. This was done by carefully comparing data in the laminar base flow to the computed profiles. If an entire profile was found to be systematically shifted in η, an appropriate correction was then applied.

3.3. *Results*

The measured base flow profiles for $R = 0$ in Fig. 7 were discussed in section 3.2. Figure 8 shows the temperature profile comparison for $R = 0.4$. Non-linear disturbance mechanisms, the immediate precursors of transition farther downstream, are known in other flows to cause an outward diffusion, or thickening of the boundary layer [1, 12]. The elevated temperature level measured near $\eta = 2.0$ may indicate this effect. The anomalous behavior of the hot film during this test makes it impossible to distinguish between linear and non-linear effects on velocity.

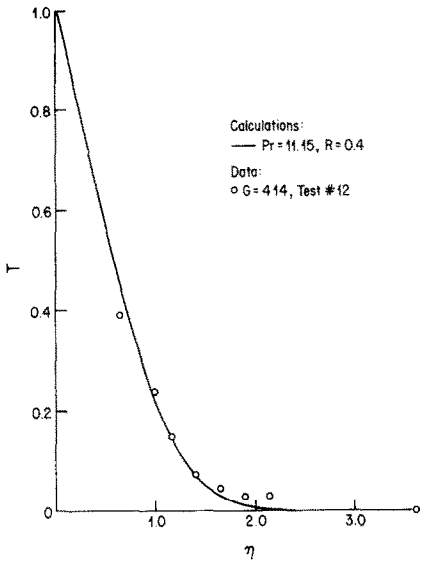

FIG. 8. Computed base flow temperature profile for $R = 0.4$, $Pr = 11.15$. Data points are the results of test 12.

The disturbance amplitude and amplification curves in Figs. 9–11 and 15 are taken from the computations [7] for an isothermal surface and $R = 0$. Figures 9 and 10 are the disturbance velocity and temperature amplitude profiles across the boundary region. The curves are for the listed values of G downstream along the constant frequency path $B = 0.36$. This is the frequency of the disturbance component which is amplified most rapidly downstream. The data points are small disturbances occurring in the laminar region, for both $R = 0$ and $R = 0.1$. The general agreement is very good for both values of R. The scatter near the outer maximum, in the large η region, arises because the velocity ratio v/u is no longer small. The hot film probe senses the resultant 2-dim. velocity vector, which is different from u.

The frequencies of those disturbances are plotted on the stability plane for $R = 0$ in Fig. 11. Average values are also indicated by the solid symbols. The data for R

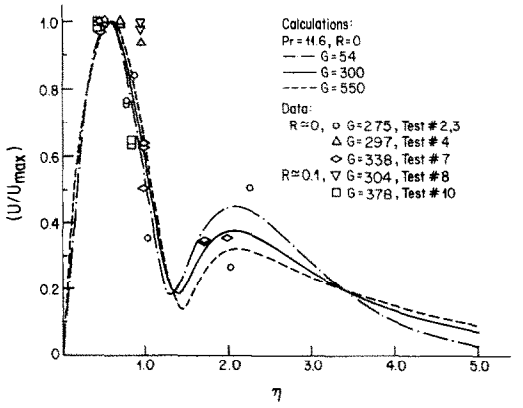

FIG. 9. Velocity disturbance amplitude profiles for $R = 0$, and several values of G, computed along a constant frequency path $B = 0.36$. Data points are linear disturbance amplitudes recorded in the laminar region, for both $R \simeq 0$ and $R \simeq 0.1$.

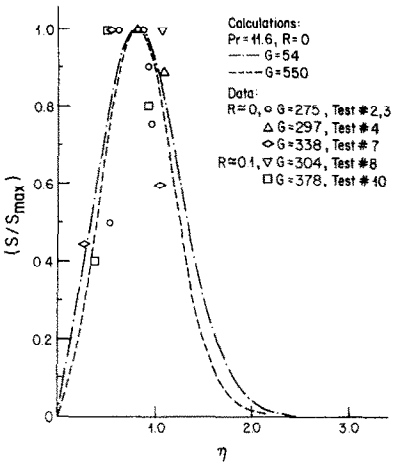

FIG. 10. Temperature disturbance amplitude profiles for $R = 0$, and two values G, computed along a constant frequency path $B = 0.36$. Data points are linear disturbance amplitudes recorded in the laminar region, for both $R \simeq 0$ and $R \simeq 0.1$.

$= 0$ lie at a frequency slightly higher than the calculated favored frequency. The range of frequencies which arose at each G location is broader than found in warmer water [1].

For the $R = 0.1$ data, the frequencies lie closer to, and also below, the favored frequency path for $R = 0$. Again, the band is broader than that observed in warmer water. This is consistent with the results in ref. [7], where it was concluded that the frequency favoring mechanism does not operate as sharply for cold water as for warm water.

The calculated stability plane for $R = 0.4$, in terms of the dimensionless frequency parameter B vs G, is shown in Fig. 12. In these coordinates, constant frequency paths are straight horizontal lines. The data point plotted at $G = 414$ is an average value. The vertical bar indicates the spread of the frequencies which arose there. As previously discussed, the hot film output drift was severe for these particular measurements. A part of the frequency band is due to this effect. Only one data point was obtained at $G = 448$. The band of the data at two values of G at $R \simeq 0.4$, are seen to lie slightly above the favored frequency.

Both Figs. 11 and 12 indicate that the first measurable disturbances occurred downstream at about the $A = 4$ amplification contour, for all values of R studied. This is in agreement with assumptions made in the preliminary design calculations carried out for the experimental surface [9].

Mean temperature distribution data are plotted for $R \simeq 0$ in Fig. 13 and for $R \simeq 0.1$ in Fig. 14. The calculated mean flow, for $R = 0$, is also shown on both figures. In Fig. 13, the data at $G = 338$ and $G = 378$ fit the calculated base flow profile closely. However, for $G = 417$, higher values are found at the outer edge of the thermal boundary region. In fact, some intermittent burst activity was detected at $G = 378$. A considerable amount was present at $G = 417$. This deviation around $\eta = 2.0$, is a clear indication of a boundary region

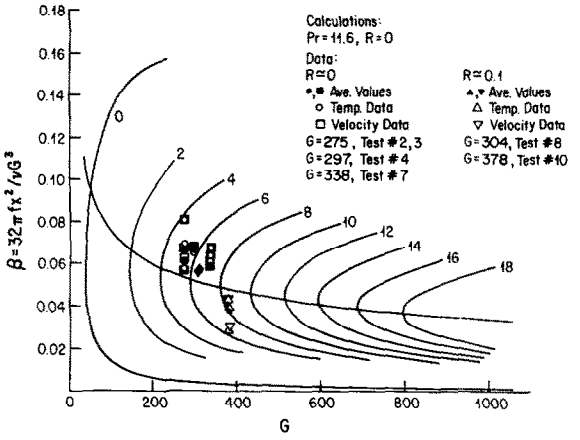

FIG. 11. Stability plane with amplification rate contours, computed for $R = 0$. Data points are the 'principal' frequencies corresponding to the linear data of Figs. 9 and 10.

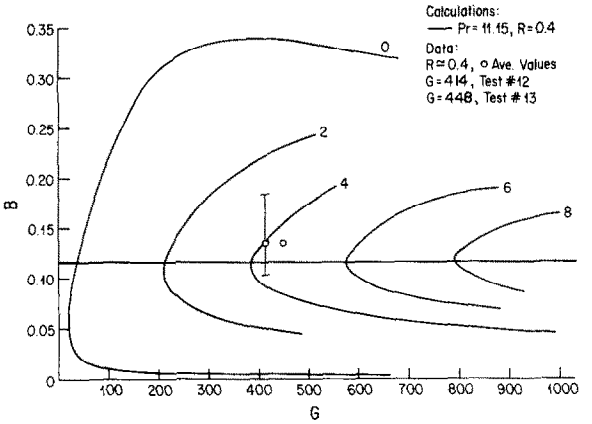

FIG. 12. Stability plane with amplification contours computed for $R = 0.4$. Data points are disturbance frequencies recorded in tests 12 and 13.

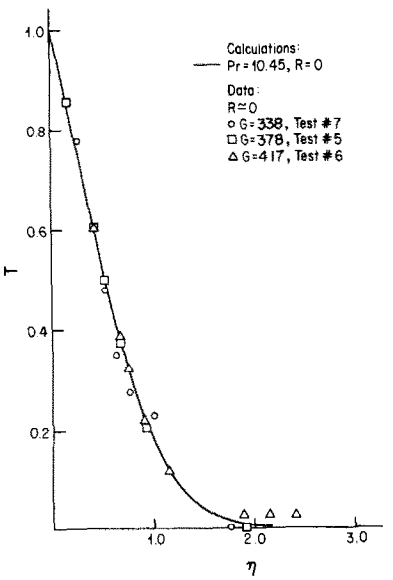

FIG. 13. Computed base flow temperature profile for $R = 0$, $Pr = 10.45$. Data points are from test indicated.

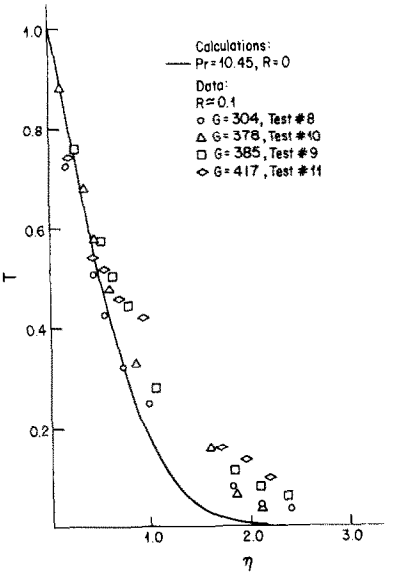

FIG. 14. Computed base flow temperature profiles for $R = 0$, $Pr = 10.45$. Data points are from tests indicated, for $R \simeq 0.1$.

thickening process, characteristic of both incipient non-linear mechanisms and the transition regime.

The measurements for $R \simeq 0.1$ for four values of G in Fig. 14, show a much greater difference. The data for $G = 304$ and $G = 378$ are very similar in trend. No bursts were detected at these locations. The disagreement with the curve could be entirely due to the consequences of non-linear disturbance growth. A small amount of burst activity was observed at $G = 385$, and a large amount at $G = 417$. Thus, the deviation of the data from the laminar profile increases with burst frequency, that is, with the progression of transition.

The kinetic energy flux parameter E, from ref. [1] and the parameter Q_{BT}, from ref. [2], to correlate beginning of transition, are given in Appendix 1. Table 1 lists the values of E and Q_{BT} for the four tests during which bursts were observed. Previous studies indicated that E and Q_{BT} lay in the following ranges, $12.9 < E < 24.0$ and $379 < Q_{BT} < 541$, for the onset of transition. These ranges cover the new data as well as all previous data for water. The specific measurements in ref. [1], in room temperature water, indicated single values of $E = 13.6$ and $E = 15.2$ for the beginning of velocity and thermal transition, respectively. Measurements in a pressurized gas (N_2) [2] yielded a single value $Q_{BT} = 290$ for the beginning of transition. These matters are summarized in Table 1 in ref. [1] and in Table 2 in ref. [2].

The tabulated values of E and Q_{BT} determined in these measurements are in good agreement with the ranges given above. Test 11 exhibited the most vigorous burst activity and, correspondingly, has the largest values for E and Q_{BT}. Test 9 showed the least vigorous activity and has one of the smallest values. Tests 5 and 9 had a very similar level of burst activity and have essentially the same values for Q_{BT}.

On the basis of the present data, in all flows containing bursts, the beginning of velocity and thermal transition occurred almost simultaneously. However, the velocity bursts were found to be slightly more 'advanced' than the temperature bursts. They were slightly more irregular in appearance than the corresponding temperature bursts, although still of approximately the same frequency. This is seen by comparing the velocity and temperature bursts shown in the traces in Figs. 6 (b) and (c).

There are three remaining downstream categories of disturbance frequencies to be discussed: predominant, large non-linear, and small non-linear frequencies. Data points for these, for $R \simeq 0$ and $R \simeq 0.1$, are shown on the stability plane for $R = 0$, in Fig. 15, for $G = 378$, 385 and 417. The points represent all three disturbance categories. Each point shown is an average taken across the boundary layer. The bars indicate the total extent of the frequency variations encountered at each G. The differences between temperature and velocity disturbance frequencies were very small, and perhaps arose only through measurement and interpretation errors. The results were therefore combined. Comparing the data at $R \simeq 0$ to the linear theory path, it is apparent that many disturbance components have arisen at a higher frequency than the favored frequency. They also continue higher downstream. Thus, when compared to the linear range results of Fig. 11, the range of frequencies is seen to have broadened downstream.

The data for $R \simeq 0.1$ are similar in some respects. However, disturbances also arise slightly below the favored frequency, and persist downstream. The frequency band spreads downstream, although the disturbances remain closer to the favored frequency than for $R \simeq 0$. For the two tests at $G = 417$, the disturbances were moved vigorous for $R \simeq 0.1$ than for $R \simeq 0$. They appeared to amplify more quickly downstream.

3.4. *Conclusions*

This new experiment concerning disturbances and transition of a buoyancy induced flow in cold water adjacent to a vertical surface required very careful design and construction to obtain a constant temperature test surface condition, as described in section 2. Linear stability calculations had determined the stability conditions for $Pr = 11.16$, $R = 0$, and $Pr = 11.15$, $R = 0.4$. In the experimental disturbance behavior was measured for t_0 and t_∞ conditions for which $R = 0, 0.1$ and 0.4. The temperature difference $(t_0 - t_\infty)$ was held to $\sim 5.0°C$, during all tests.

Temperature and velocity measurements were made with a fine thermocouple probe and a hot film anemometer. The velocities expected and encountered in this study were smaller than those usually measured with a hot film. Extreme care was necessary to reduce error in the course of taking measurements. However, the base flow calculations and resulting measurements are in excellent agreement.

Use of a hot film anemometer in regions where the fluid temperature variation includes t_m presents special problems. In experiments at $R = 0.1$, i.e. $t_0 \simeq 9.0°C$ and $t_\infty \simeq 3.3°C$, a slight drift, or meandering of the anemometer output occurred in the coldest areas of

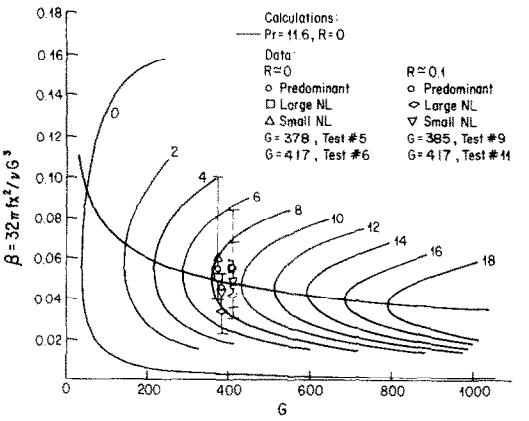

FIG. 15. Stability plane with amplification rate contours, computed for $R = 0$. Data points illustrate results in the categories of predominant, large NL, and small NL frequencies, for the tests indicated, for both $R \simeq 0$, and $R \simeq 0.1$.

the boundary layer. At $R = 0.4$, $t_0 \simeq 6.6°C$ and $t_\infty \simeq 2.3°C$, a region where much of the boundary layer temperature is below t_m, this behavior was severe. In addition, $R = 0.4$ is a downflow circumstance. However, the hot wire calibration procedure simulated an upflow circumstance. In that configuration, in a boundary layer, the flow would reinforce, rather than oppose, the plume flow generated by the probe. The velocity of that plume was of a significant magnitude compared to that of many boundary layer flows in cold water. A separate downflow calibration and different operating procedure is clearly necessary to obtain good velocity data in such circumstances. Only frequencies, not disturbance amplitudes, were processed from the data for $R = 0.4$.

Measured disturbance amplitude data, for $R \simeq 0$ and $R \simeq 0.1$, agree well with the computed linear disturbance profiles. The selective frequency amplification mechanism was both calculated and measured to be less sharp in cold water than has been observed in warm water. This is consistent with the observations [7] in cold water, for a uniform surface flux condition.

For $R \simeq 0$, disturbance activity begins and propagates downstream at a frequency slightly higher than the calculated favored frequency. As transition begins and proceeds, the frequency band broadens. For $R \simeq 0.1$, the earliest disturbance frequencies are calculated slightly below the favored frequency. They remain closer to the calculated trend, downstream, than those for $R \simeq 0$.

Disturbances for $R \simeq 0.1$ for $G = 417$, were of large amplitude and more vigorous than those for $R \simeq 0$, for the same value of G. This is in agreement with linear theory, which predicts more rapid downstream disturbance amplification.

Thermal and velocity transition were found to occur simultaneously, in agreement with the results [7] in cold water. It was noted, however, that the velocity disturbances were slightly more 'developed' or irregular in appearance than the corresponding temperature disturbances under the same conditions. Average temperature and velocity frequencies were essentially the same. This result, as well as the simultaneous velocity and thermal transition differ somewhat from the observations reported [1] in room temperature water.

Bursts, signaling the beginning of transition, were observed during four test conditions. The conditions under which bursts arose correspond with the predicted transition parameters E and Q_{BT}, defined in Appendix 1. However, there is some shift upstream, indicating the presence of an enhanced amplification mechanism operating in cold water.

Acknowledgements—The authors wish to acknowledge research support from the National Science Foundation during this investigation under grants CME 77-21641 and MEA 8200613.

REFERENCES

1. Y. Jaluria and B. Gebhart, On transition mechanisms in vertical natural convection flow, *J. Fluid Mech.* **66,** 309–337 (1974).
2. R. L. Mahajan and B. Gebhart, An experimental determination of transition limits in a vertical natural convection flow adjacent to a surface, *J. Fluid Mech.* **91,** 131–154 (1979).
3. C. E. Polymeropoulos and B. Gebhart, Incipient instability in free convection laminar boundary layers, *J. Fluid Mech.* **30,** 225–239 (1967).
4. C. P. Knowles and B. Gebhart, The stability of the laminar natural convection boundary layer, *J. Fluid Mech.* **34,** 657–686 (1968).
5. R. P. Dring and B. Gebhart, A theoretical investigation of disturbance amplification in external laminar natural convection, *J. Fluid Mech.* **34,** 551–564 (1968).
6. C. A. Heiber and B. Gebhart, The stability of vertical natural convection boundary layers: expansions of Prandtl number, *J. Fluid Mech.* **49,** 577–592 (1971).
7. Z. H. Qureshi, Stability and measurements of fluid and thermal transport in vertical buoyancy induced flows in cold water, doctoral dissertation, SUNYAB, Buffalo, New York (1980).
8. B. Gebhart and J. C. Mollendorf, A new density relation for pure and saline water, *Deep-Sea Res.* **24,** 831–848 (1977).
9. J. M. Higgins, Stability of buoyancy induced flow of water near the density extremum, adjacent to a vertical, isothermal surface, doctoral dissertation, SUNYAB, Buffalo, New York (1981).
10. H. Shaukatullah and B. Gebhart, Effect of flow direction on calibration of hot-film anemometers at low velocities, *Trans. Am. Soc. Mech. Engrs,* Series C, *J. Heat Transfer,* **100,** 381–382 (1978).
11. Y. Joshi, Pressure stress and viscous dissipation effects in natural convection and an experimental investigation of line source plumes in cold water. Master's thesis, SUNYAB, Buffalo, New York (1981).
12. T. Audunson and B. Gebhart, Secondary mean motions arising in a buoyancy-induced flows, *Int. J. Heat Mass Transfer* **19,** 737–750 (1976).

APPENDIX 1

USE OF THE KINETIC ENERGY FLUX PARAMETER E, AND BEGINNING OF TRANSITION PARAMETER Q_{BT}

The experimental results in water [1] have shown definitely that transition events are not correlated merely in terms of the Grashof number. The data show a better correlation through use of the kinetic energy flux parameter

$$E = G^* \left(\frac{\nu^2}{gx^3}\right)^{2/15}.$$

In this case, the following parameters are defined

$$G^* = (4+q)\left[\frac{1}{(4+q)}\frac{g\alpha x^3}{\nu^2}\left(\frac{q''x}{k}\right)^q\right]^{1/(4+q)},$$

and $q'' = k\Delta TG/4x\,[-T'(0)]$, for an isothermal surface.

The further measurements in a gas [2] indicated that the 'beginning of transition parameter', Q_{BT}, correlates a wider range of properties, and fits data well for both liquids and gases. The parameter is defined as follows:

$$Q_{BT} = \left(\frac{q''}{g\mu}\right)^{1/5}\left(\frac{gx^3}{\nu^2}\right)^{2/15}.$$

A summary of values of E and Q_{BT} for tests which exhibited 'bursts' in this study are presented in Table 1.

MESURE DE LA CROISSANCE DE L'INSTABILITE ET DE LA PERTURBATION DANS LES ECOULEMENTS NATURELS VERTICAUX DANS L'EAU FROIDE

Résumé—On développe une étude expérimentale de la stabilité d'un écoulement induit par les forces d'Archimède dans l'eau froide, adjacent à une surface isotherme verticale. Une surface a été construite pour réaliser la condition de surface isotherme. L'expérience est proche de l'extrémum de densité, aux valeurs $R = 0, 0{,}1$ et 0,4, avec une différence de température $(t_0 - t_\infty)$ limitée à 5°C. Des calculs de stabilité linéaire ont été effectués pour ces conditions. L'écoulement de base et la perturbation de température et de vitesse sont mesurés avec une sonde à thermocouple et un anémomètre à film chaud. Pour les deux circonstances $R = 0$ et $R = 0{,}1$, l'amplitude de la perturbation mesurée s'accorde bien avec les profils calculés linéairement. Pour $R = 0$, l'activité de la perturbation apparait et se propage en aval à une fréquence légèrement plus grande que celle prédite par des calculs linéaires pour être plus rapidement amplifiée, ou "favorisée" en fréquence. Pour $R = 0{,}1$ les fréquences caractéristiques mesurées sont légèrement au dessous de la fréquence calculée favorable. Quand la transition apparait, on trouve un domaine de fréquence élargi. Des perturbations à $R = 0{,}1$ apparaissent plus tôt et sont plus vigoureuses que celles observées à $R = 0$, en accord avec la théorie linéaire.

Des problèmes de mesure sont rencontrès pour $R = 0$, et $t_0 \cong 6{,}6$, $t_\infty \cong 2{,}3$°C. Pour ces conditions, la partie externe de la couche limite thermique est en dessous de la température extrémale, avec une force de volume se renversant. Les fréquences mesurées de perturbation sont légèrement plus élevées que la fréquence calculée.

Une activité de bouffées annonce le début de la transition dans plusieurs essais. La situation et la vigueur de cette activité correspondent aux valeurs des paramètres E et O_{BT} proposés par Jaburia et Gebhart [1], et par Mahajan et Gebhart [2]. Les valeurs expérimentales de E et Q_{BT} déterminées ici sont légèrement plus faibles quque celles précédemment rapportées. Ceci indique la présence d'une instabilité accrue et d'un mécanisme d'amplification dans l'eau froide, en terme des paramètres qui apparaissent dans E et Q_{BT}.

MESSUNGEN DER INSTABILITÄT UND DES ANWACHSENS VON STÖRUNGEN IN SENKRECHTEN AUFTRIEBSBEDINGTEN STRÖMUNGEN IN KALTEM WASSER

Zusammenfassung—Eine experimentelle Untersuchung der Stabilität von durch Auftrieb bedingten Strömungen von kaltem Wasser an einer senkrechten isothermen Oberfläche wurde durchgeführt. Eine große Oberfläche wurde so entworfen und ausgeführt, daß die isotherme Oberflächen bedingung zu erfüllen war. Das Experiment wurde in der Nähe des Dichtemaximums durchgeführt, bei Parameterwerten von $R = 0$; 0,1 und 0,4 bei einer maximalen Temperaturdifferenz $(t_0 - t_\infty)$ von 5°C (vgl. Tafel 1). Zuvor waren lineare Stabilitätsberechnungen für diese Bedingungen durchgeführt worden. Die Temperaturen und Geschwindigkeiten der Grundströmung sowie der Störungen wurden mit einer empfindlichen Thermoelementsonde bzw. einem Hitzdrahtanemometer gemessen. Für die aufwärts gerichteten Strömungen bei $R = 0$ und $R = 0{,}1$ stimmten die gemessenen Werte der Störungsamplituden gut mit den linear berechneten Störungsprofilen überein. Für $R = 0$ treten Störungsaktivitäten zuerst auf und pflanzen sich stromabwärts fort mit einer Frequenz, die etwas höher liegt als die sich nach linearen Berechnungen am schnellsten verstärkende oder "bevorzugte" Frequenz. Für $R = 0{,}1$ liegen die gemessenen charakteristischen Frequenzen etwas unterhalb der berechneten bevorzugten Frequenz. Im Verlauf des instationären Vorgangs wird ein sich ausdehnender Bereich von Frequenzen gemessen. In Übereinstimmung mit der linearen Theorie entwickeln sich bei $R = 0{,}1$ die Störungen früher und stärker als bei $R = 0$.

Bei $R = 0{,}4$ traten systematische Meßprobleme auf, wobei $t_0 \approx 6{,}6$°C und $t_\infty \approx 2{,}3$°C betrugen. Unter diesen Bedingungen liegt die Temperatur des äußeren Teils der thermischen Grenzschicht unterhalb der Temperatur des Extremums, wobei die Auftriebskraft in entgegengesetzte Richtung wirkt. Die gemessenen Störungsfrequenzen lagen etwas höher als die berechneten bevorzugten Frequenzen.

Bei mehreren der durchgeführten Versuche wurde der Beginn des instationären Verlaufs durch Berstaktivität angezeigt. Die Lage und Stärke dieser Aktivität stimmt mit den entsprechenden Parameterwerten E und Q_{BT} gut überein, die von Jaluria und Gebhart [1] und Mahajan und Gebhart [2] vorgeschlagen wurden. Die experimentell ermittelten Werte für E und Q_{BT}, die hier bestimmt wurden, lagen etwas niedriger als die früher angegebenen. Dies deutet auf erhöhte Instabilitäts- und Verstärkungsmechanismen in kaltem Wasser hin, die mit ähnlichen Parametern wie denen, die in E and Q_{BT} auftreten, beschrieben werden können.

ЭКСПЕРИМЕНТАЛЬНОЕ ИССЛЕДОВАНИЕ УСТОЙЧИВОСТИ И РОСТА ВОЗМУЩЕНИЙ В ВЕРТИКАЛЬНЫХ СВОБОДНОКОНВЕКТИВНЫХ ВОСХОДЯЩИХ ПОТОКАХ В ХОЛОДНОЙ ВОДЕ

Аннотация—Выполнено экспериментальное исследование устойчивости индуцированного подъемными силами течения воды у вертикальной изотермической поверхности. Для получения изотермических условий на поверхности была изготовлена пластина большой протяженности. Эксперимент проводился в условиях вблизи экстремума плотности при значениях параметра R, равных 0; 0,1 и 0,4, и разности температур $(t_0 - t_\infty)$, не превышающей 5°C (см. Табл. 1). Расчеты по линейной теории устойчивости для этих условий были выполнены ранее. Течение и распределение температур и скорости возмущений у основания пластины измерялись миниатюрной термопарой и пленочным термоанемометром. Для случаев $R = 0$ и $R = 0{,}1$ измеренные амплитуды возмущений хорошо согласуются с результатами расчета профилей возмущения по линейной теории. При $R = 0$ возникающее возмущение распространяется вниз по потоку с частотой, несколько превышающей расчетную, а затем эта частота очень быстро увеличивается и далее не изменяется. При $R = 0{,}1$ измеренные значения характеристических частот несколько ниже расчетной. По мере развития переходного процесса обнаружено увеличение диапазона частот возмущений. Возмущения при $R = 0{,}1$ возникают быстрее и являются более интенсивными, чем при $R = 0$, что соответствует линейной теории.

Некоторые затруднения представили систематические измерения при $R = 0{,}4$, когда $t_0 \approx 6{,}6$ и $t_\infty \approx 2{,}3$ C. В этих условиях температура внешней части теплового пограничного слоя ниже экстремальной, причем отмечается обращение действия выталкивающей силы. Измеренные значения частот возмущения оказались несколько выше расчетной частоты.

Начало переходного процесса в нескольких из выполненных опытов сопровождалось появлением выбросов. Их местоположение и интенсивность соответствуют значениям расчетных параметров E и Q_{BT}, предложенных Жалурия и Гебхартом [1], а также Махаджаном и Гебхартом [2]. Полученные в данной работе экспериментальные значения E и Q_{BT} оказались несколько ниже определенных ранее. Это указывает на наличие значительной неустойчивости в холодной воде.